Dzyaloshinskii-Moriya interaction in magnetoferroelectric superlattices: Spin waves and skyrmions

I. F. Sharafullin,[1,2] M. Kh. Kharrasov,[2] and H. T. Diep[1]

[1]*Laboratoire de Physique Théorique et Modélisation Université de Cergy-Pontoise, CNRS, UMR 8089, 2 Avenue Adolphe Chauvin, 95302 Cergy-Pontoise, Cedex, France*
[2]*Bashkir State University, 32, Validy str, 450076, Ufa, Russia*

We study in this paper effects of Dzyaloshinskii-Moriya (DM) magnetoelectric coupling between ferroelectric and magnetic layers in a superlattice formed by alternate magnetic and ferroelectric films. Magnetic films are films of simple cubic lattice with Heisenberg spins interacting with each other via an exchange J and a DM interaction with the ferroelectric interface. Electrical polarizations of ± 1 are assigned at simple cubic lattice sites in the ferroelectric films. We determine the ground-state (GS) spin configuration in the magnetic film. In zero field, the GS is periodically noncollinear and in an applied field **H** perpendicular to the layers, it shows the existence of skyrmions at the interface. Using the Green's function method, we study the spin waves (SW) excited in a monolayer and also in a bilayer sandwiched between ferroelectric films, in zero field. We show that the DM interaction strongly affects the long-wavelength SW mode. We calculate also the magnetization at low temperature T. We use next Monte Carlo simulations to calculate various physical quantities at finite temperatures such as the critical temperature, the layer magnetization, and the layer polarization, as functions of the magnetoelectric DM coupling and the applied magnetic field. Phase transition to the disordered phase is studied in detail.

I. INTRODUCTION

Nonuniform spin structures, which are quite interesting by themselves, became the subject of close attention after the discovery of electrical polarization in some of them [1]. The existence of polarization is possible due to the inhomogeneous magnetoelectric effect, namely, that electrical polarization can occur in the region of magnetic inhomogeneity. It is known that the electric polarization vector is transformed in the same way as the combination of the magnetization vector and the gradient of the magnetization vector, meaning that these values can be related by the proportionality relation. In Ref. [2] it was found that in a crystal with cubic symmetry, the relationship between electrical polarization and inhomogeneous distribution of the magnetization vector has the following form:

$$\mathbf{P} = \gamma \chi_e [\mathbf{M} \cdot (\nabla \cdot \mathbf{M}) - (\mathbf{M} \cdot \nabla) \cdot \mathbf{M}], \tag{1}$$

where γ is the magnetoelectric coefficient and χ_e the permittivity. In noncollinear structures, the microscopic mechanism of the coupling of polarization and the relative orientation of the magnetization vectors is based on the interaction of Dzyaloshinskii-Moriya (DM) [3–5]. The corresponding term in the Hamiltonian is

$$H_{\mathrm{DM}} = \mathbf{D}_{i,j} \cdot \mathbf{S_i} \times \mathbf{S_j}, \tag{2}$$

where $\mathbf{S_i}$ is the spin of the ith magnetic ion, and $\mathbf{D}_{i,j}$ is the Dzyaloshinskii-Moriya vector. The vector $\mathbf{D}_{i,j}$ is proportional to the vector product $\mathbf{R} \times \mathbf{r_{i,j}}$ of the vector $\mathbf{R}$ which specifies the displacement of the ligand (for example, oxygen) and the unit vector $\mathbf{r_{i,j}}$ along the axis connecting the magnetic ions i

and j [see Fig. 1(a)]. We write

$$\mathbf{D}_{i,j} \propto \mathbf{R} \times \mathbf{r_{i,j}}. \tag{3}$$

Thus, the Dzyaloshinskii-Moriya interaction connects the angle between the spins and the magnitude of the displacement of nonmagnetic ions. In some micromagnetic structures, all ligands are shifted in one direction, which leads to the appearance of macroscopic electrical polarization [see Fig. 1(b)]. By nature, this interaction is a relativistic amendment to the indirect exchange interaction, and is relatively weak [6]. In the case of magnetically ordered matter, the contribution of the Dzyaloshinskii-Moriya interaction to the free energy can be represented as Lifshitz antisymmetric invariants containing spatial derivatives of the magnetization vector. In analogy, the vortex magnetic configuration can be stable via Skyrme mechanism [7]. Skyrmions were theoretically predicted more than 20 years ago as stable micromagnetic structures [8]. The idea came from nuclear physics, where the elementary particles were represented as vortex configurations of continuous fields. The stability of such configurations was provided by the "Skyrme mechanism," the components in Lagrangians containing antisymmetric combinations of spatial derivatives of field components [9]. For a long time skyrmions have been the subject only of theoretical studies. In particular, it was shown that such structures can exist in antiferromagnets [10] and in magnetic metals [11]. In the latter case, the model included the possibility of changing the magnitude of the magnetization vector and spontaneous emergence of the skyrmion lattice without the application of external magnetic field. A necessary condition for the
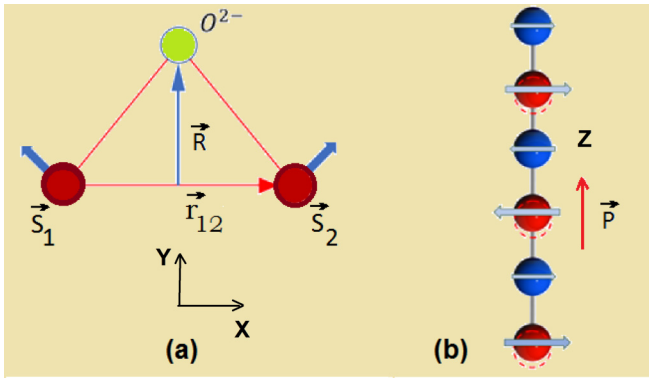
FIG. 1. (a) Schema of Dzyaloshinskii-Moriya interaction, spins are in the xy plane; (b) microscopic mechanisms of creation of electric spontaneous polarization **P** due to displacements of atoms (red) in the same direction z.

existence of skyrmions in bulk samples was the absence of an inverse transformation in the crystal magnetic symmetry group. Diep *et al.* [12] have studied a crystal of skyrmions generated on a square lattice using a ferromagnetic exchange interaction and a Dzyaloshinskii-Moriya interaction between nearest neighbors under an external magnetic field. They have shown that the skyrmion crystal has a hexagonal structure which is shown to be stable up to a temperature T_c where a transition to the paramagnetic phase occurs and the dynamics of the skyrmions at $T < T_c$ follows a stretched exponential law. In Ref. [11] it was shown that the most extensive class of candidates for the detection of skyrmions includes the surfaces and interfaces of magnetic materials, where the geometry of the material breaks the central symmetry and, therefore, can lead to the appearance of chiral interactions similar to the Dzyaloshinskii-Moriya interaction. In addition, skyrmions are two-dimensional (2D) solitons, the stability of which is provided by the local competition of short-range interactions exchange and Dzyaloshinskii-Moriya interactions [12,13]. The idea of using skyrmions in memory devices nowadays is reduced to the information encoding using the presence or absence of a skyrmion in certain area of the material. A numerical simulation of the creation and displacement of skyrmions in thin films was carried out in Ref. [14] using a spin-polarized current. The advantage of skyrmions with respect to the domain boundaries in such magnetic memory circuits (e.g., racetrack memory, see Ref. [15]) is the relatively low magnitude of the currents required to move the skyrmions along the "track." For the first time, skyrmions were experimentally detected in the MnSi helimagnet [16]. Below the Curie temperature in MnSi spins are aligned in helicoidal or conical structure (the field was applied along the [100] axis), depending on the magnitude of the applied magnetic field. Similar experimental results were obtained for the compound $Fe_{1-x}Co_xSi$, $x = 0.2$ [17]. The investigation of $Fe_{0.5}Co_{0.5}Si$ made it possible to take the next important step in the study of skyrmions: to directly observe them using Lorentz electron microscopy [18]. The dependence of the stability of the skyrmion lattice on the sample thickness of FeGe was studied in more detail in Ref. [19]. Studies have confirmed that the thinner was the film, the greater

was the "stability region" of skyrmions. Skyrmions as the most compact isolated micromagnetic objects are of great practical interest as memory elements [13]. The stability of skyrmions [12] can make the memory on their basis non-volatile, and low control currents will reduce the cost of rewriting compared to similar technologies based on domain boundaries. In Refs. [20,21] magnetic and electrical properties of the skyrmion lattice were studied in the multiferroic Cu_2OSeO_3. It has been shown that that energy consumption can be minimized by using the electric field to control the micromagnetic structures. It is worth noting that the multiferroics $BaFe_{12-x-0.05}Sc_xMg_{0.05}O_{19}$ may also have a skyrmion structure [22,23]. The manipulations with skyrmions were first demonstrated in the diatomic PdFe layer on the iridium substrate, and the importance of this achievement for the technology of information storing is difficult to overestimate: it makes possible to write and read the individual skyrmions using a spin-polarized tunneling current [24]. In Ref. [25], the possibility of the nucleation of skyrmions by the electric field by means of an inhomogeneous magnetoelectric effect was established.

Recent studies are focused on the interface-induced skyrmions. Therefore, the superstructures naturally lead to the interaction of skyrmions on different interfaces, which has unique dynamics compared to the interaction of the same-interface skyrmions. In Ref. [26], a theoretical study of two skyrmions on two-layer systems was carried using micromagnetic modeling, as well as an analysis based on the Thiele equation, which revealed a reaction between them, such as the collision and a bound-state formation. The dynamics sensitively depends on the sign of DM interaction, i.e., the helicity, and the skyrmion numbers of two skyrmions, which are well described by the Thiele equation. In addition, the colossal spin-transfer-torque effect of bound skyrmion pair on antiferromagnetically coupled bilayer systems was discovered. In Ref. [27] the study of the Thiele equation was carried for current-induced motion in a skyrmion lattice through two soluble models of the pinning potential.

We consider in this paper a superlattice composed of alternate magnetic films and ferroelectric films. The aim of this paper is to propose a model for the coupling between the magnetic film and the ferroelectric film by introducing a DM-like interaction. It turns out that this interface coupling gives rise to noncollinear spin configurations in zero applied magnetic field and to skyrmions in a field **H** applied perpendicularly to the films. Using the Green's function method, we study spin-wave excitations in zero field of a monolayer and a bilayer. We find that the DM interaction affects strongly the long-wavelength mode. Monte Carlo simulations are carried out to study the phase transition of the superlattice as functions of the interface coupling strength.

The paper is organized as follows. Section II is devoted to the description of our model and the determination of the ground-state spin configuration with and without applied magnetic field. Section III shows the results obtained by Monte Carlo simulations for the phase transition in the system as a function of the interface DM coupling. In Sec. IV we show the results of the Green's function technique in zero field for a monolayer and a bilayer. Concluding remarks are given in Sec. V.
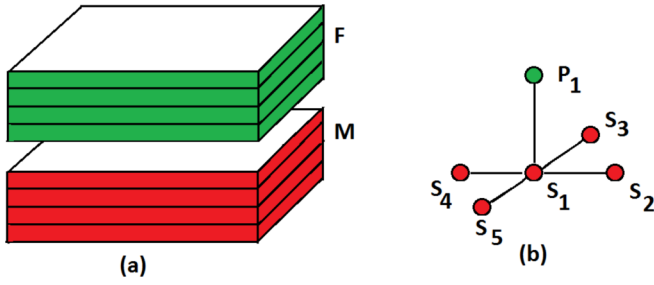
FIG. 2. (a) The superlattice composed of alternately a ferroelectric layer indicated by F and a magnetic layer indicated by M; (b) a polarization P_1 at the interface interacts with five spins in the magnetic layer. See text for expression.

II. MODEL AND GROUND STATE

A. Model

Consider a superlattice composed of alternate magnetic and ferroelectric films [see Fig. 2(a)]. Both have the structure of simple cubic lattice of the same lattice constant, for simplicity. The Hamiltonian of this multiferroic superlattice is expressed as

$$\mathcal{H} = H_m + H_f + H_{mf}, \tag{4}$$

where H_m and H_f are the Hamiltonians of the ferromagnetic and ferroelectric subsystems, respectively, while H_{mf} is the Hamiltonian of magnetoelectric interaction at the interface between two adjacent films.

We describe the Hamiltonian of the magnetic film with the Heisenberg spin model on a simple cubic lattice:

$$H_m = -\sum_{i,j} J_{ij}^m \mathbf{S}_i \cdot \mathbf{S}_j - \sum_i \mathbf{H} \cdot \mathbf{S}_i, \tag{5}$$

where $\mathbf{S}_i$ is the spin on the ith site, $\mathbf{H}$ is the external magnetic field, $J_{ij}^m > 0$ the ferromagnetic interaction parameter between a spin and its nearest neighbors (NN), and the sum is taken over NN spin pairs. We consider $J_{ij}^m > 0$ to be the same, namely, J^m, for spins everywhere in the magnetic film. The external magnetic field $\mathbf{H}$ is applied along the z axis which is perpendicular to the plane of the layers. The interaction of the spins at the interface will be given below.

For the ferroelectric film, we suppose for simplicity that electric polarizations are Ising-type vectors of magnitude 1, pointing in the $\pm z$ direction. The Hamiltonian is given by

$$H_f = -\sum_{i,j} J_{ij}^f \mathbf{P}_i \cdot \mathbf{P}_j - \sum_i E^z P_i^z, \tag{6}$$

where $\mathbf{P}_i$ is the polarization on the ith lattice site, $J_{ij}^f > 0$ the interaction parameter between NN, and the sum is taken over NN sites. Similar to the ferromagnetic subsystem we will take the same $J_{ij}^f = J^f$ for all ferroelectric sites. We apply the external electric field $\mathbf{E}$ along the z axis.

We suppose the following Hamiltonian for the magnetoelectric interaction at the interface:

$$H_{mf} = \sum_{i,j,k} J_{ijk}^{mf} \mathbf{D}_{i,j} \cdot [\mathbf{S_i} \times \mathbf{S_j}]. \tag{7}$$

In this expression, $J_{ijk}^{mf} \mathbf{D}_{i,j}$ plays the role of the DM vector which is perpendicular to the xy plane. Using Eqs. (2) and (3), one has

$$\mathbf{D}_{i,j} = \mathbf{R} \times \mathbf{r}_{i,j},$$
$$\mathbf{D}_{j,i} = \mathbf{R} \times \mathbf{r}_{j,i} = -\mathbf{D}_{i,j}. \tag{8}$$

Now, let us define for our model

$$J_{ijk}^{mf} = J_{i,j}^{mf} P_k, \tag{9}$$

which is the DM interaction parameter between the electric polarization $\mathbf{P}_k$ at the interface ferroelectric layer and the two NN spins $\mathbf{S}_i$ and $\mathbf{S}_j$ belonging to the interface ferromagnetic layer. Hereafter, we suppose $J_{i,j}^{mf} = J^{mf}$ independent of (i, j). Selecting $\mathbf{R}$ in the xy plane perpendicular to $\mathbf{r}_{i,j}$ (see Fig. 1), we can write $\mathbf{R} \times \mathbf{r}_{i,j} = a\mathbf{z} \, e_{i,j}$ where $e_{i,j} = -e_{j,i} = 1$, a is a constant, and $\mathbf{z}$ the unit vector on the z axis.

It is worth at this stage to specify the nature of the DM interaction to avoid a confusion often seen in the literature. The term $[\mathbf{S}_i \times \mathbf{S}_j]$ changes its sign with the permutation of i and j, but the whole DM interaction defined in Eq. (2) does not change its sign because $D_{i,j}$ changes its sign with the permutation as seen in Eq. (3). Note that if the whole DM interaction is antisymmetric, then when we perform the lattice sum, nothing of the DM interaction remains in the Hamiltonian. This explains why we need the coefficient $e_{i,j}$ introduced above and present in Eq. (10).

We collect all these definitions we write H_{mf} in a simple form

$$
\begin{aligned}
H_{mf} &= \sum_{i,j,k} J^{mf} P_k \, (\mathbf{R} \times \mathbf{r}_{i,j}) \cdot [\mathbf{S_i} \times \mathbf{S_j}] \\
&= \sum_{i,j,k} J^{mf} P_k \, e_{i,j} \mathbf{z} \cdot [\mathbf{S_i} \times \mathbf{S_j}] \\
&= \sum_{i,j,k} J^{mf} \, e_{i,j} \, \mathbf{P}_k \cdot [\mathbf{S_i} \times \mathbf{S_j}], \tag{10}
\end{aligned}
$$

where the constant a is absorbed in J^{mf}.

As seen in Eq. (10), the coefficient of the interface coupling is proportional to $\langle P_k \rangle$ which depends on T. If $\langle P_k \rangle$ becomes zero before the loss of skyrmion texture, we will not see the latter. Therefore, we have chosen the polarization of the Ising type with ferroelectric interaction parameter J^f in a way that its transition temperature is higher than that of the magnetic part. Note that the magnetic transition is driven by the competition between T and the magnetic texture (skyrmions) which is a result of the competition between J, the DM interaction (namely, $\langle P_k \rangle$) and field H.

We note that the DM interaction is taken only between NN spin. If we choose the DM vector $\mathbf{D}$ perpendicular to the xy plane, then the DM interaction energy is minimum when the spins are in the xy plane because $\mathbf{D}$ is parallel to $[\mathbf{S}_i \times \mathbf{S}_j]$. One can choose any orientation for $\mathbf{D}$ but in that case to have the minimum energy the plane containing $\mathbf{S}_i$ and $\mathbf{S}_j$ should be perpendicular to $\mathbf{D}$: the spins are not in the xy plane, making the spin configuration analysis difficult.

The superlattice and the interface interaction are shown in Fig. 2. A polarization at the interface interact with five spins on the magnetic layer according to Eq. (10), for example [see

Fig. 2(b)],

$$
J^{mf}\mathbf{P_1} \cdot [e_{1,2}(\mathbf{S_1} \times \mathbf{S_2}) + e_{1,3}(\mathbf{S_1} \times \mathbf{S_3})
$$
$$
+ e_{1,4}(\mathbf{S_1} \times \mathbf{S_4}) + e_{1,5}(\mathbf{S_1} \times \mathbf{S_5})]. \tag{11}
$$

Since we suppose $\mathbf{P}_k$ is a vector of magnitude 1 pointing along the z axis, namely, its z component is $P_k^z = \pm 1$, we will use hereafter P_k^z for electric polarization instead of $\mathbf{P}_k$. From Eq. (10), we see that the magnetoelectric interaction J^{mf} favors a canted spin structure. It competes with the exchange interaction J of H_m which favors collinear spin configurations. Usually, the magnetic or ferroelectric exchange interaction is the leading term in the Hamiltonian, so that in many situations the magnetoelectric effect is negligible. However, in nanofilms of superlattices the magnetoelectric interaction is crucial for the creation of noncollinear long-range spin order.

Note that the hypothesis that $\mathbf{P}_k$ is in the z direction in order to have the polarization proportional to the DM vector [Eqs. (7)–(10)]. The DM vector is taken in the z direction in order to have spins in the magnetic layers lying in the xy plane, in the absence of an applied field (see Secs. II B 1 and IV). The polarization is in addition supposed of the Ising type since in this paper, this assumption allows us to have the DM vector in a fixed direction z. The assumption is justified by the fact that in ferroelectric materials, if atoms are displaced in the same direction, it gives rise to a spontaneous polarization in that direction as illustrated in Fig. 1(b).

B. Ground state

1. Ground state in zero magnetic field

Let us analyze the structure of the ground state (GS) in zero magnetic field. Since the polarizations are along the z axis, the interface DM interaction is minimum when $\mathbf{S_i}$ and $\mathbf{S_j}$ lie in the xy interface plane and perpendicular to each other. However, the ferromagnetic exchange interaction among the spins will compete with the DM perpendicular configuration. The resulting configuration is noncollinear. We will determine it below, but at this stage, we note that the ferroelectric film has always polarizations along the z axis even when interface interaction is turned on.

Let us determine the GS spin configurations in magnetic layers in zero field. If the magnetic film has only one monolayer, the minimization of H_{mf} in zero magnetic field is done as follows. By symmetry, each spin has the same angle θ with its four NN in the xy plane. The energy of the spin $\mathbf{S}_i$ gives the relation between θ and J^m:

$$
E_i = -4J^m S^2 \cos\theta + 8J^{mf} P^z S^2 \sin\theta, \tag{12}
$$

where $\theta = |\theta_{i,j}|$ and care has been taken on the signs of $\sin\theta_{i,j}$ when counting NN, namely, two opposite NN have opposite signs, and the opposite coefficient e_{ij}, as given in Eq. (11). Note that the coefficient 4 of the first term is the number of in-plane NN pairs, and the coefficient 8 of the second term is due to the fact that each spin has 4 coupling DM pairs with the NN polarization in the upper ferroelectric plane, and 4 with the NN polarization of the lower ferroelectric plane (we are in the case of a magnetic monolayer). The minimization of E_i

yields, taking $P^z = 1$ in the GS and $S = 1$,

$$
\frac{dE_i}{d\theta} = 0 \implies \frac{-2J^{mf}}{J^m} = \tan\theta \implies \theta = \arctan\left(-\frac{2J^{mf}}{J^m}\right). \tag{13}
$$

The value of θ for a given $\frac{-2J^{mf}}{J^m}$ is precisely what is obtained by the numerical minimization of the energy. We see that when $J^{mf} \to 0$, one has $\theta \to 0$, and when $J^{mf} \to -\infty$, one has $J^{mf} \to \pi/2$, as it should be. Note that we will consider in this paper $J^{mf} < 0$ so as to have $\theta > 0$. The above relation between the angle and J^{mf} will be used in the last section to calculate the spin waves in the case of a magnetic monolayer sandwiched between ferroelectric films.

In the case when the magnetic film has a thickness, the angle between NN spins in each magnetic layer is different from that of the neighboring layer. It is more convenient using the numerical minimization method called "steepest descent method" to obtain the GS spin configuration. This method consists in minimizing the energy of each spin by aligning it parallel to the local field acting on it from its NN. This is done as follows. We generate a random initial spin configuration, then we take one spin and calculate the interaction field from its NN. We align it in the direction of this field, and take another spin and repeat the procedure until all spins are considered. We go again for another sweep until the total energy converges to a minimum. In principle, with this iteration procedure the system can be stuck in a metastable state when there is a strong interaction disorder such as in spin glasses. But for uniform, translational interactions, we have never encountered such a problem in many systems studied so far.

We use a sample size $N \times N \times L$. For most calculations, we select $N = 40$ and $L = 8$ using the periodic boundary conditions in the xy plane. For simplicity, when we investigate the effect of the exchange couplings on the magnetic and ferroelectric properties, we take the same thickness for the magnetic and ferroelectric films, namely, $L_a = L_b = 4 = L/2$. Exchange parameters between spins and polarizations are taken as $J^m = J^f = 1$ for the simulation. For simplicity, we will consider the case where the in-plane and interplane exchange magnetic and ferroelectric interactions between nearest neighbors are both positive. All the results are obtained with $J^m = J^f = 1$ for different values of the interaction parameter J^{mf}.

We investigated the following range of values for the interaction parameters J^{mf}: from $J^{mf} = -0.05$ to -6.0 with different values of the external magnetic and electric fields. We note that the steepest descent method calculates the real ground state with the minimum energy to the value $J^{mf} = -1.25$. After larger values, the angle θ tends to $\pi/2$ so that all magnetic exchange terms (scalar products) will be close to zero, the minimum energy corresponds to the DM energy. Figure 3 shows the GS configurations of the magnetic interface layer for small values of J^{mf}: $-0.1, -0.125, -0.15$. Such small values yield small values of angles between spins so that the GS configurations have ferromagnetic and noncollinear domains. Note that angles in magnetic interior layers are different but the GS configurations are of the same texture (not shown).
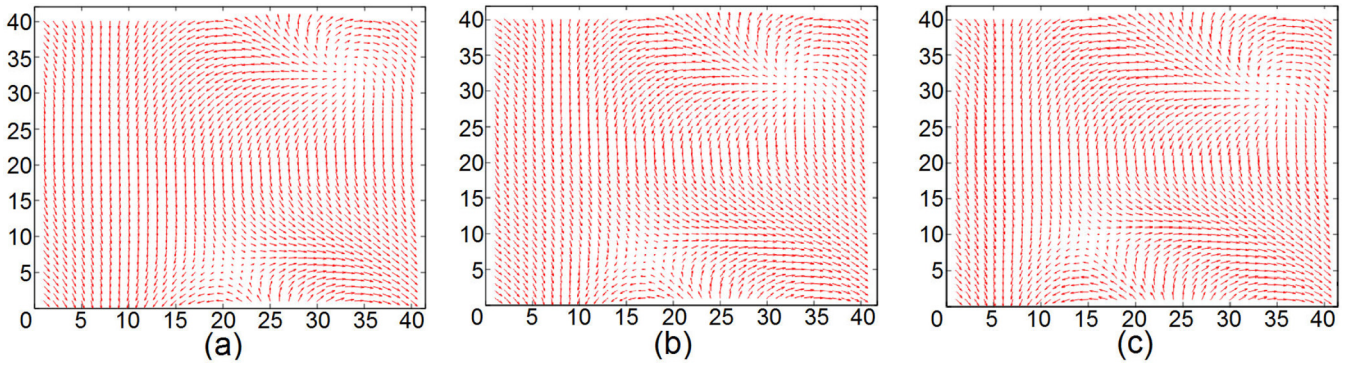
FIG. 3. GS spin configuration for weak couplings: $J^{mf} = -0.1$ (a), -0.125 (b), -0.15 (c), with $H = 0$.

For larger values of J^{mf}, the GS spin configurations have periodic structures with no more mixed domains. We show in Fig. 4 examples where $J^{mf} = -0.45$ and -1.2. Several remarks are in order:

(i) Each spin has the same turning angle θ with its NN in both x and y directions. The schematic zoom in Fig. 4(c) shows that the spins on the same diagonal (spins 1 and 2, spins 3 and 4) are parallel. This explains the structures shown in Figs. 4(a) and 4(b).

(ii) The periodicity of the diagonal parallel lines depends on the value of θ [comparing Figs. 4(a) and 4(b)]. With a large size of N, the periodic conditions have no significant effects.

2. Ground state in applied magnetic field

We apply a magnetic field perpendicular to the xy plane. As we know, in systems where some spin orientations are incompatible with the field such as in antiferromagnets, the down spins cannot be turned into the field direction without losing their interaction energy with the up spins. To preserve this interaction, the spins turn into the direction almost perpendicular to the field while staying almost parallel with each other. This phenomenon is called "spin flop" [28]. In more complicated systems such as helimagnets in a field, more complicated reaction of spins to the field was observed, leading to striking phenomena such as partial phase transition in thin helimagnetic films [29]. In the present system, there is a competition between the applied field which wants to align
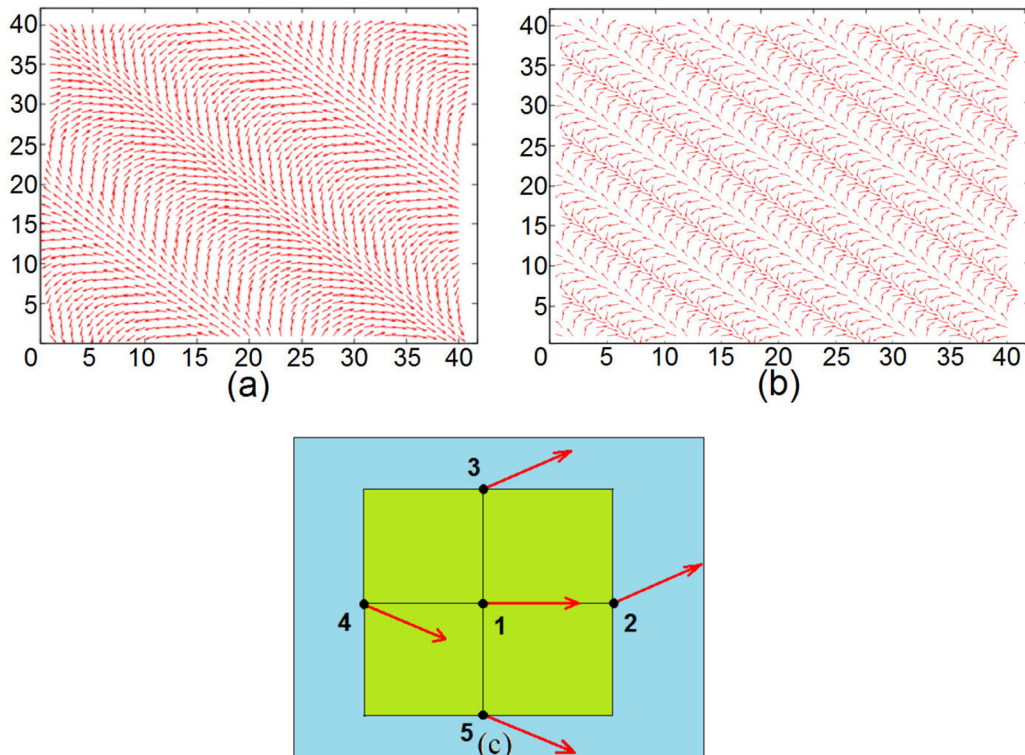

FIG. 4. GS spin configurations for $J^{mf} = -0.45$ (a), -1.2 (b), with $H = 0$. Angles between NN are schematically zoomed (c). See text for comments.
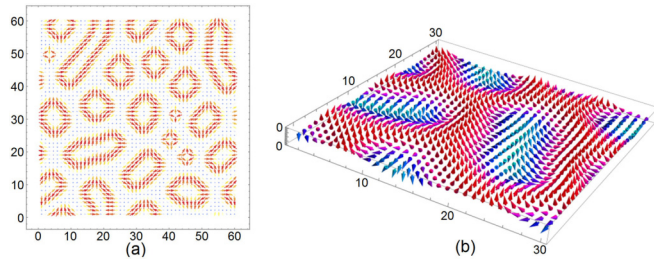
FIG. 5. GS configuration of the surface magnetic layer for (a) $J^{mf} = -1.1$ and $H = 0.1$, (b) 3D view of the surface GS configuration.

the spins along the z direction, and the DM interaction which wants the spins to be perpendicular which each other in the x plane. As a consequence, spins find a compromise which is the structure of skyrmions as shown below.

Figure 5(a) shows the ground-state configuration for $J^{mf} = -1.1$ for first (surface) magnetic layer, with external magnetic layer $H = 0.1$. Figure 5(b) shows the three-dimensional (3D) view. We can observe the beginning of the birth of skyrmions at the interface and in the interior magnetic layer.

Figure 6(a) shows the ground-state configuration for $J^{mf} = -1.1$ for first (surface) magnetic layer, with external magnetic layer $H = 0.2$. Figure 6(b) shows the 3D view. We can observe the skyrmions for the surface and interior magnetic layer. Note that the skyrmions are found here in a range of sufficiently strong interface coupling and the applied field. The skyrmions are distributed in 3D space (not on a plane) in the magnetic layer. Figure 6 shows a cut in xy plane so that the projected sizes are not uniform. We have made a single magnetic layer: in that case, skyrmions are uniform on a 2D sheet (not shown). We note that the skyrmion and antiskyrmion textures are not degenerate due to the DM asymmetry [see Eq. (10)]: choosing the direction of **P** will fix the skyrmion turning direction, i.e., $[\mathbf{S}_i \times \mathbf{S}_j]$. Changing **P** will change skyrmions into antiskyrmions or vice versa.

Figure 7 shows the GS configuration of the interface magnetic layer (top) for $J^{mf} = -1.1$, with external magnetic layer $H = 0.33$. The bottom figure shows the configurations of the second (interior) magnetic layer. We can observe skyrmions on both the interface and the interior magnetic layers.

Figure 8 shows the 3D view of the GS configuration for $J^{mf} = -1.1$, with $H = 0.33$ for the first (interface) magnetic layer and the second (interior) magnetic layer. We can observe skyrmions very pronounced for the surface layer but less
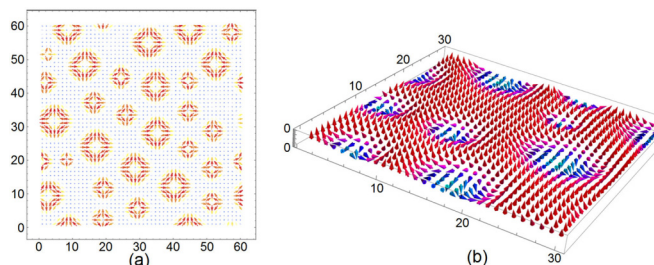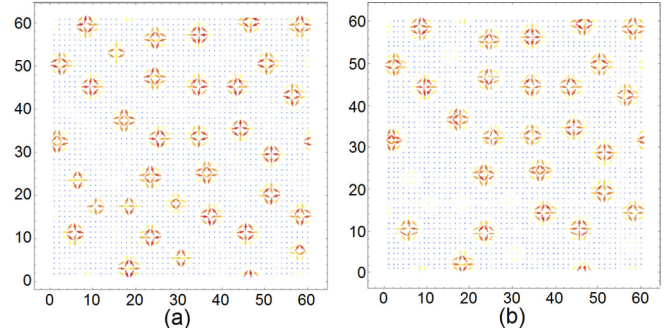

FIG. 7. (a) GS configuration for the interface magnetic layer for $J^{mf} = -1.1$ and $H = 0.33$, (b) GS configurations for the second and third magnetic layers (they are identical). See text for comments.

contrast for the interior magnetic layer. For fields stronger than $H = 0.33$, skyrmions disappear in interior layers. At strong fields, all spins are parallel to the field, thus no skyrmions anywhere.

III. MONTE CARLO RESULTS

We have used the Metropolis algorithm [30,31] to calculate physical quantities of the system at finite temperatures T. As said above, we use mostly the size $N \times N \times L$ with $N = 40$ and thickness $L = L_m + L_f = 8$ (4 magnetic layers, 4 ferroelectric layers). Simulation times are 10^5 Monte Carlo

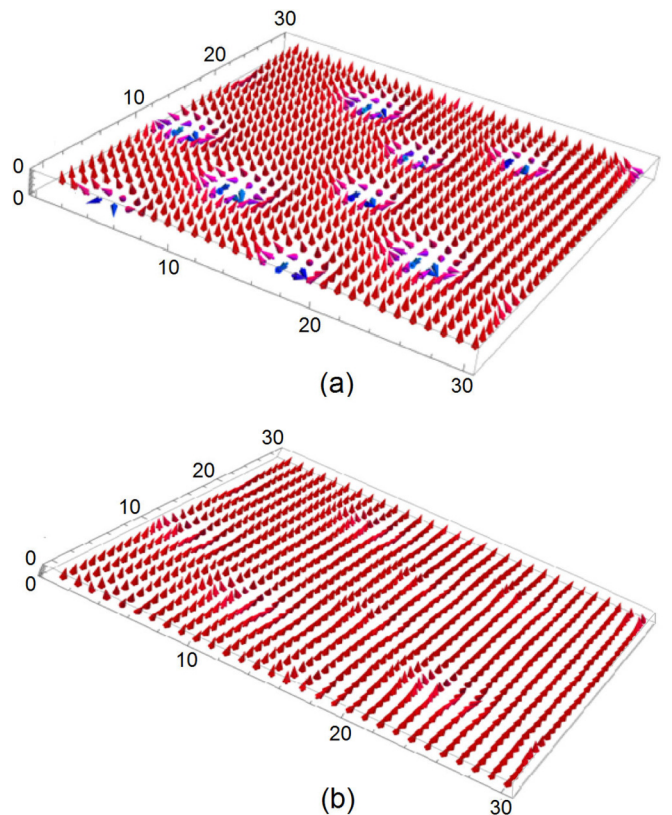FIG. 6. (a) GS configuration for the surface magnetic layer for $J^{mf} = -1.1$ and $H = 0.2$, (b) 3D view.

FIG. 8. (a) 3D view of the GS configuration of the interface, (b) 3D view of the GS configuration of the second and third magnetic layers, for J^{mf} and $H = 0.33$.

steps (MCS) per spin for equilibrating the system and 10^5 MCS/spin for averaging. We calculate the internal energy and the layer order parameters of the magnetic (M_m) and ferroelectric (M_f) films.

The order parameter $M_f(n)$ of layer n is defined as

$$M_f(n) = \frac{1}{N^2} \left\langle \left| \sum_{i \in n} P_i^z \right| \right\rangle, \quad (14)$$

where $\langle \ldots \rangle$ denotes the time average. The definition of an order parameter for a skyrmion crystal is not obvious. Taking advantage of the fact that we know the GS, we define the order parameter as the projection of an actual spin configuration at a given T on its GS and we take the time average. This order parameter of layer n is thus defined as

$$M_m(n) = \frac{1}{N^2(t_a - t_0)} \sum_{i \in n} \left| \sum_{t=t_0}^{t_a} \mathbf{S}_i(T, t) \cdot \mathbf{S}_i^0(T=0) \right|, \quad (15)$$

where $\mathbf{S}_i(T, t)$ is the ith spin at the time t, at temperature T, and $\mathbf{S}_i(T = 0)$ is its state in the GS. The order parameter $M_m(n)$ is close to 1 at very low T where each spin is only weakly deviated from its state in the GS. $M_m(n)$ is zero when every spin strongly fluctuates in the paramagnetic state. The above definition of $M_m(n)$ is similar to the Edward-Anderson (EA) order parameter used to measure the degree of freezing in spin glasses [32]. The EA order parameter, by definition, is calculated as follows. We follow each spin during the time. If it is frozen, then its time average is not zero. If it strongly fluctuates with time evolution, then its time average is zero. To calculate the overall degree of freezing, it suffices to add the square of each spin's time average. In doing so, we see that the EA order parameter does not express the nature of ordering, but only the degree of freezing.

In general, when the GS has several degenerate configurations such as the all-up and the all-down spin configurations in a ferromagnetic system of Ising spins, the system chooses one of the two when T tends to 0. The coexistence of several phases is not tolerated in such a case because the resulting energy is higher than that of a pure one (due to walls). However, in frustrated systems where one can construct a ground state by random stacking of frustrated units, one does not have a long-range ordering. In this paper, we wish to follow the evolution of the system ordering from $T = 0$, so we have to compare the configuration at temperature T at the time t with the GS we have selected to do the slow heating. That was what we did: we compare the actual configuration obtained by slowly heating the selected GS by projecting it on the selected GS [see Eq. (15)]. There are several possibilities: (i) if the spin structure is not stable when $T \neq 0$, $M_m(n)$ goes to zero with time, this is the case of the Kosterlitz-Thouless (XY spins in 2D with NN interaction); (ii) if the spin structure is frozen or ordered (spin glasses (SG), ferromagnets,...), $M_m(n)$ is not zero at low T. In our case of skyrmion structure, we have observed the second case, namely, the GS is stable up to a finite T.

If the system makes a global rotation during the simulation, then $\sum_{t=t_0}^{t_a} \mathbf{S}_i(T, t) \cdot \mathbf{S}_i^0(T = 0) = 0$ for a long-time average. But, the length of this runtime depends on the nature of ordering and the size of the system used in simulations.
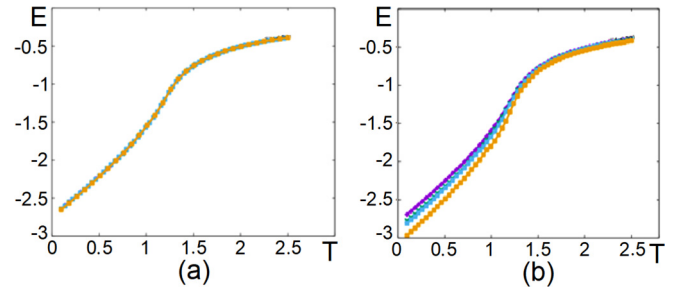

FIG. 9. Energy of the magnetic film versus temperature T for (a) $J^{mf} = -0.1$, $J^{mf} = -0.125$, $J^{mf} = -0.15$, $J^{mf} = -0.2$ (all the lines are the same, see text for comments); (b) $J^{mf} = -0.45$ (purple line), $J^{mf} = -0.75$ (green line), $J^{mf} = -0.85$ (blue line), and $J^{mf} = -1.2$ (gold line), without an external magnetic field.

For large disordered systems such as SG and complicated noncollinear extended skyrmion structures, the global rotation may be forbidden or the time to realize it is out of reach in MC simulations. To see if a global rotation is realized or not, we have to make a finite-time scaling to deduce properties at the infinite time. This is very similar in spirit with the finite-size scaling used to deduce properties at the infinite crystal size. We have previously performed a finite-time scaling for the 2D skyrmion crystal [33]. In that work, we have used the same order parameter as Eq. (15). We have seen that skyrmions need much more than 10^6 MC steps per spin to relax to equilibrium. The order parameter follows a stretched exponential law as in SG and stabilized at nonzero values for $T < T_c$ at the infinite time. If there is a global rotation, we would not have nonzero values of $M_m(n)$ for $T < T_c$ at the infinite time. We note that in this work, as in Ref. [33], we have made a very slow heating of a selected GS and we did not observe a global rotation.

Note that the counting of topological charges around each skyrmion is numerically possible. In that case, the charge number evolves with T and goes to zero at the phase transition. The procedure is equivalent to projecting the skyrmion spin texture on its GS. We have chosen the projection one. The total order parameters M_m and M_f are the sum of the layer order parameters, namely, $M_m = \sum_n M_m(n)$ and $M_f = \sum_n M_f(n)$.

In Fig. 9 we show the dependence of energy of the magnetic film versus temperature, without an external magnetic field, for various values of the interface magnetoelectric interaction: in Fig. 9(a) for weak values $J^{mf} = -0.1$, $J^{mf} = -0.125$, $J^{mf} = -0.15$, $J^{mf} = -0.2$, and in Fig. 9(b) for stronger values $J^{mf} = -0.45$, $J^{mf} = -0.75$, $J^{mf} = -0.85$, $J^{mf} = -1.2$.

As said in the GS determination, when J^{mf} is weak, the GS is composed with large ferromagnetic domains at the interface (see Fig. 3). Interior layers are still ferromagnetic. The energy therefore does not vary with weak values of J^{mf} as seen in Fig. 9(a). The phase transition occurs at the curvature change, namely, maximum of the derivative or maximum of the specific heat $T_c^m \simeq 1.25$. Note that the energy at $T = 0$ is equal to -2.75 by extrapolating the curves in Fig. 9(a) to $T = 0$. This value is just the sum of energies of the spins across the layers: 2 interior spins with 6 NN, 2 interface spins with 5 NN. The energy per spin is thus (in ferromagnetic state) $E = -(2 \times 6 + 2 \times 5)/(4 \times 2) = -2.75$ (the factor 2
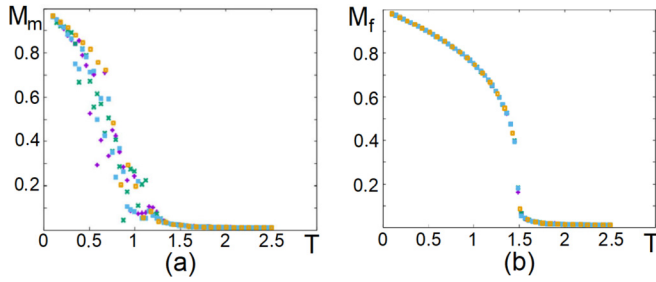
FIG. 10. (a) Order parameter of the magnetic film M_m versus T; (b) order parameter of the ferroelectric film M_f versus T, for $J^{mf} = -0.1$ (purple dots), $J^{mf} = -0.125$ (green dots), $J^{mf} = -0.15$ (blue dots), $J^{mf} = -0.2$ (gold dots), without an external magnetic field.

in the denominator is to remove the bond double counting in a crystal).

For stronger values of J^{mf}, the curves shown in Fig. 9(b) indicate a deviation of the ferromagnetic state due to the noncollinear interface structure. Nevertheless, we observe the magnetic transition at almost the same temperature, namely, $T_c^m \simeq 1.25$. It means that spins in interior layers dominate the ordering.

We show in Fig. 10 the total order parameters of the magnetic film M_m and the ferroelectric film M_f versus T for various values of the parameter of the magnetoelectric interaction $J^{mf} = -0.1, -0.125, -0.15, -0.2$ and for $J^{mf} = -0.45, -0.75, -0.85, -1.2$, without an external magnetic field. Several remarks are in order:

(i) For the magnetic film, M_m shows strong fluctuations but we still see that all curves fall to zero at $T_c^m \simeq 1.25$. These fluctuations come from nonuniform spin configurations and also from the nature of the Heisenberg spins in low dimensions [34].

(ii) For the ferroelectric film, M_f behaves very well with no fluctuations. This is due to the Ising nature of electric polarizations supposed in the present model. The ferroelectric film undergoes a phase transition at $T_c^f \simeq 1.50$.

(iii) There are thus two transitions, one magnetic and one ferroelectric, separately. The magnetic transition occurs at a lower temperature. We know that in bulk crystals the transition temperature is approximatively proportional to $1/n$ where n is the component number of the spin: $n = 3$ for the Heisenberg spin, $n = 1$ for the Ising spin [35,36]. The fact that the ferroelectric transition occurs at a higher temperature observed in Fig. 10(b) is understood. The weak coupling with the magnetic film makes the two transition temperatures separately. Between T_c^m and T_c^f, the superlattice is partially disordered: the magnetic part is disordered while the ferroelectric part is ordered. The partial disorder has been observed in many systems, for example, the surface layer of a thin film can become disordered at a low temperature while the bulk is still ordered [37]. One can also mention the partial phase transition in helimagnets in a field [29].

We show in Fig. 11 the order parameters of the magnetic and ferroelectric films at strong values of J^{mf} as functions of T, in zero field. We observe that the stronger $|J^{mf}|$ is, the lower T_c^m becomes. This is understood by the discussion given below Eq. (13) for a monolayer: the stronger $|J^{mf}|$ makes the
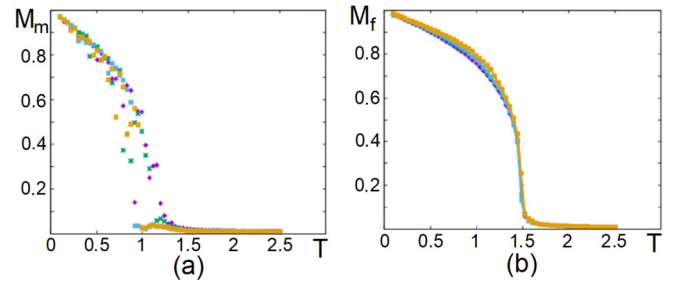

FIG. 11. (a) Order parameter of the magnetic film versus T; (b) order parameter of the ferroelectric film versus T for $J^{mf} = -0.45$ (purple dots), $J^{mf} = -0.75$ (green dots), $J^{mf} = -0.85$ (blue dots), and $J^{mf} = -1.2$ (gold dots), without an external magnetic field.

larger angle θ. In the case of many magnetic layers shown in Fig. 11, the larger angle causes a stronger competition with the collinear ferromagnetic interaction of the interior layers. This enhanced competition gives rise to the destruction of the ordering at a lower temperature.

We examine the field effects now. Figure 12 shows the order parameter and the energy of the magnetic film versus T, for various values of the external magnetic field. The interface magnetoelectric interaction is $J^{mf} = -1.2$. Depending on the magnetic field, the noncollinear spin configuration survives up to a temperature between 0.5 and 1 (for $H = 0$). After the transition, spins align themselves in the field direction, giving a large value of the order parameter [Fig. 12(a)]. The energy shows a sharp curvature change only for $H = 0$, meaning that the specific heat is sharp only for $H = 0$ and broadened more and more with increasing H.

We consider now the case of very strong interface couplings.

Figure 13(a) shows the magnetic order parameter versus T. The purple and green lines correspond to M for $J^{mf} = -2.5$ with $H^z = 1.0$ and 1.5, respectively; the blue and gold lines correspond to M for $J^{mf} = -6$ with $H^z = 0$ and 1. These curves indicate first-order phase transitions at $T_c^m = 1.05$ for ($J^{mf} = -2.5$, $H^z = 1$) (purple), at $T_c^m = 1.12$ for ($J^{mf} = -2.5$, $H^z = 1.5$) (green), and at $T_c^m = 1.25$ for ($J^{mf} = -6$, $H^z = 1$) (blue). In the case of zero field, namely ($J^{mf} = -6$, $H^z = 0$) (gold), one has a first-order phase transitions occurring at $T_c = 2.30$.
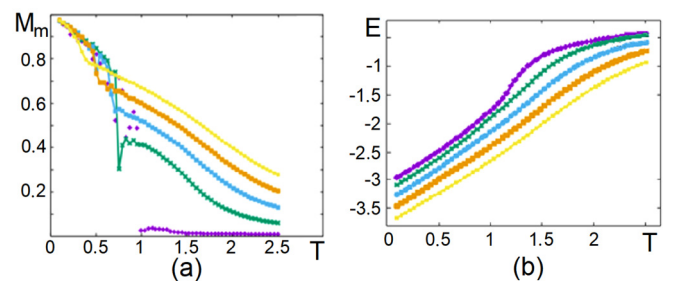

FIG. 12. (a) Temperature dependence of (a) the magnetic order parameter; (b) the magnetic energy for $H = 0$ (purple dots), $H = 0.25$ (green line), $H = 0.5$ (blue line), $H = 0.75$ (gold line), $H = 1$ (yellow line). The interface magnetoelectric interaction is $J^{mf} = -1.2$.
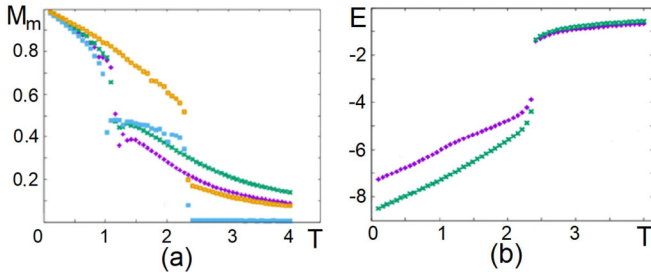
FIG. 13. (a) Order parameter of magnetic film versus T. The purple and green dots correspond to M for ($J^{mf} = -2.5$, $H^z = 1$) and ($J^{mf} = -2.5$, $H^z = 1.5$), blue and gold dots correspond to M for ($J^{mf} = -6$, $H^z = 1$) and ($J^{mf} = -6$, $H^z = 0$). (b) Energies of magnetic (purple dots) and ferroelectric (green dots) subsystems versus T for ($J^{mf} = -6$, $H = 0$).
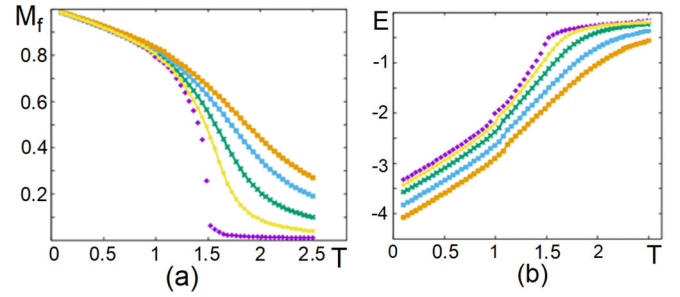

FIG. 14. (a) Order parameter and (b) energy of ferroelectric film, versus temperature for $E = 0$ (purple dots), $E = 0.25$ (green line), $E = 0.5$ (blue line), $E = 0.75$ (gold line), $E = 1$ (yellow line). The interface magnetoelectric interaction is $J^{mf} = -1.2$.

Let us discuss about the nature of the transition shown in Fig. 13(a). When $H \neq 0$, the first transition at low temperature ($T \simeq 1.05$–1.25) is due to the destruction of the skyrmion structure. After this transition, the z-spin components being not zero under an applied field come close to zero only at high T ($\simeq 2.3$). This is not a phase transition because the z components will never be zero in a field if J^{mf} is not so strong. When J^{mf} is very strong ($J^{mf} = -6$, blue data points), the DM interaction is so strong that the spins will lie in the xy plane in spite of H: we see that the z-spin components are zero after the loss of the ferroelectric ordering at $T \simeq 2.3$. Note that when $H = 0$ (gold data points), there is no skyrmion, the spin configuration is chiral (helical) as shown in Sec. III. The single transition to the paramagnetic phase occurs at $T \simeq 2.3$ where the chiral ordering and the ferroelectric ordering are lost at the same time [see Fig. 13(b)].

Figure 13(b) shows the magnetic (purple) and ferroelectric (green) energies versus T for ($J^{mf} = -6$, $H^z = 0$). One sees the discontinuities of these curves at $T_c \simeq 2.3$, indicating the first-order transitions for both magnetic and ferroelectric at the same temperature. In fact, with such a strong J^{mf} the transitions in both magnetic and ferroelectric films are driven by the interface, this explains the same T_c for both. The first-order transition observed here can be understood because the present system is a frustrated system due to the competing interactions. So far, all frustrated noncollinear spin systems have been found possessing a first-order transition (see Ref. [38] and references in Ref. [39]).

Let us show the effect of an applied electric field. For the ferroelectric film, polarizations are along the z axis so that an applied electric field **E** along this direction will remove the phase transition: the order parameter never vanishes when $E \neq 0$, similar to the case of a ferromagnet in an applied magnetic field. This is seen in Fig. 14. Note that the energy has a sharp change of curvature for $E = 0$ indicating a transition, other energy curves with $E \neq 0$ do not show a transition. One notices some anomalies at $T \sim 1$–1.1 which are due to the effect of the magnetic transition in this temperature range.

IV. SPIN WAVES IN ZERO FIELD

We have shown in the previous section Monte Carlo results for the phase transition in our superlattice model. Here, let us

show theoretically spin waves (SW) excited in the magnetic film in zero field, in some simple cases. The method we employ is the Green's function technique for noncollinear spin configurations which has been shown to be efficient for studying low-T properties of quantum spin systems such as helimagnets [40] and systems with a DM interaction [41].

In this section, we consider the same Hamiltonian supposed in Eqs. (4)–(10) but with quantum spins of amplitude $\frac{1}{2}$. As seen in the previous section, the spins lie in the xy planes, each on its quantization local axis lying in the xy plane (quantization axis being the ζ axis, see Fig. 15).

Expressing the spins in the local coordinates, one has

$$\mathbf{S}_i = S_i^{\xi_i}\hat{\xi}_i + S_i^{\eta_i}\hat{\eta}_i + S_i^{\zeta_i}\hat{\zeta}_i, \tag{16}$$

$$\mathbf{S}_j = S_j^{\xi_j}\hat{\xi}_j + S_j^{\eta_j}\hat{\eta}_j + S_j^{\zeta_j}\hat{\zeta}_j, \tag{17}$$

where the i and j coordinates are connected by the rotation

$$\hat{\xi}_j = \cos\theta_{ij}\hat{\zeta}_i + \sin\theta_{ij}\hat{\xi}_i,$$

$$\hat{\zeta}_j = -\sin\theta_{ij}\hat{\zeta}_i + \cos\theta_{ij}\hat{\xi}_i, \quad \hat{\eta}_j = \hat{\eta}_i,$$

where $\theta_{ij} = \theta_i - \theta_j$ being the angle between $\mathbf{S}_i$ and $\mathbf{S}_j$.

As we have seen above, the GS spin configuration for one monolayer is periodically noncollinear. For two-layer magnetic film, the spin configurations in two layers are identical by symmetry. However, for thickness larger than 2, the interior layer has angles different from that on the interface layer. It is not our purpose to treat that case though it is possible to do so
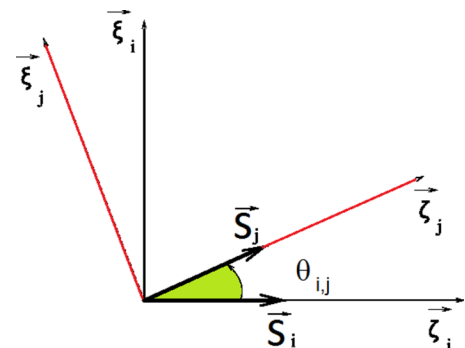

FIG. 15. The spin quantization axes of $\mathbf{S}_i$ and $\mathbf{S}_j$ are $\hat{\zeta}_i$ and $\hat{\zeta}_j$, respectively, in the xy plane.
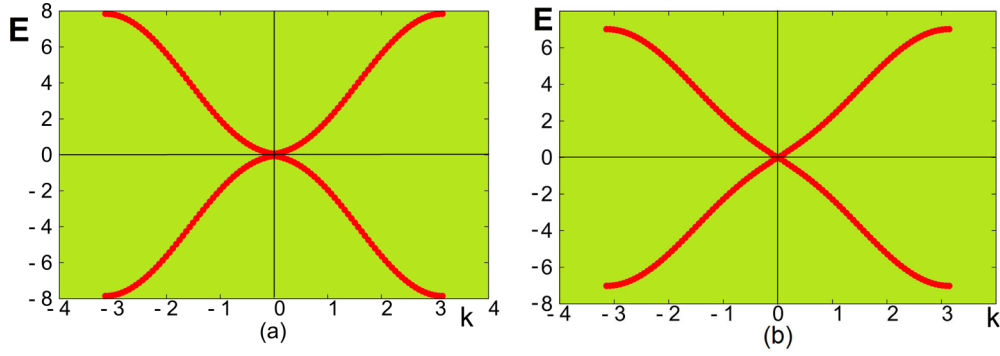
FIG. 16. Spin-wave energy $E(k)$ versus k ($k \equiv k_x = k_z$) for (a) $\theta = 0.3$ radian and (b) $\theta = 1$ in 2D at $T = 0$. See text for comments.

using the method described in Ref. [41]. We rather concentrate ourselves in the case of a monolayer in this section.

In this paper, we consider the case of spin one-half ($S = \frac{1}{2}$). Expressing the total magnetic Hamiltonian $\mathcal{H}_M = \mathcal{H}_m + \mathcal{H}_{mf}$ in the local coordinates [41]. Writing $\mathbf{S}_j$ in the coordinates $(\hat{\xi}_i, \hat{\eta}_i, \hat{\zeta}_i)$, one gets the following exchange Hamiltonian from Eqs. (4)–(10):

$$
\mathcal{H}_M = -\sum_{\langle i,j \rangle} J^m \left\{ \frac{1}{4}(\cos\theta_{i,j} - 1)(S_i^+ S_j^+ + S_i^- S_j^-) \right.
$$

$$
+ \frac{1}{4}(\cos\theta_{i,j} + 1)(S_i^+ S_j^- + S_i^- S_j^+)
$$

$$
+ \frac{1}{2}\sin\theta_{i,j}(S_i^+ + S_i^-)S_j^z - \frac{1}{2}\sin\theta_{i,j}S_i^z(S_j^+ + S_j^-)
$$

$$
\left. + \cos\theta_{i,j}S_i^z S_j^z \right\} + \frac{D}{4}\sum_{\langle i,j \rangle}\left[(S_i^+ + S_i^-)(S_j^+ + S_j^-)|\sin\theta_{i,j}|\right.
$$

$$
\left. + 4S_i^z S_j^z |\sin\theta_{i,j}| \right], \tag{18}
$$

where $D = J^{mf} P^z$. Note that $P^z = 1$ in the GS. At finite T we replace P^z by $\langle P^z \rangle$. In the above equation, we have used standard notations of spin operators for easier recognition when using the commutation relations in the course of calculation, namely,

$$
\begin{aligned}
\left(S_i^{\xi_i}, S_i^{\eta_i}, S_i^{\zeta_i}\right) &\to \left(S_i^x, S_i^y, S_i^z\right), \\
\left(S_j^{\xi_j}, S_j^{\eta_j}, S_j^{\zeta_j}\right) &\to \left(S_j^x, S_j^y, S_j^z\right),
\end{aligned} \tag{19}
$$

where we understand that S_i^x is in fact $S_i^{x_i}$ and so on.

Note that the sinus terms of $\mathcal{H}_m$, the third line of Eq. (18), are zero when summed up on opposite NN unlike the sinus term of the DM Hamiltonian H_{mf} [Eq. (10)] which remains thanks to the choice of the DM vectors for opposite directions in [41].

A. Monolayer

In two dimensions (2D) there is no long-range order at finite temperature (T) for isotropic spin models with short-range interaction [34]. Therefore, to stabilize the ordering at finite T it is useful to add an anisotropic interaction to stabilize the magnetic long-range ordering when the wave vector vanishes [see Fig. 16(a) for instance]. It is known that in 2D or in very thin films, the integrands to calculate $\langle M \rangle$ at a finite T [see Eq. (38)] diverges as $k\,dk/k^2$ (since $E => k^2$

for the ferromagnetic mode when $k => 0$) while in 3D this is $k^2 dk/k^2$ as $k => 0$ (no problem of divergence). In MC simulations shown in the previous section, the statistical average was done using stochastic random configurations generated by statistical probability (no possible mode of $k = 0$). So, we do not encounter such a mathematical divergence as in the SW calculation.

We use the following anisotropy between $\mathbf{S}_i$ and $\mathbf{S}_j$ which stabilizes the angle determined above between their local quantization axes S_i^z and S_j^z:

$$
\mathcal{H}_a = -\sum_{\langle i,j \rangle} K_{i,j} S_i^z S_j^z \cos\theta_{i,j}, \tag{20}
$$

where $K_{i,j}$ is supposed to be positive, small compared to J^m, and limited to NN. Hereafter, we take $K_{i,j} = K$ for NN pair in the xy plane, for simplicity. The total magnetic Hamiltonian $\mathcal{H}_M$ is finally given by (using operator notations)

$$
\mathcal{H}_M = \mathcal{H}_m + \mathcal{H}_{mf} + \mathcal{H}_a. \tag{21}
$$

We now define the following two double-time Green's functions in the real space:

$$
\begin{aligned}
G_{i,j}(t,t') &= \langle\langle S_i^+(t); S_j^-(t')\rangle\rangle \\
&= -i\theta(t - t')\langle[S_i^+(t), S_j^-(t')]\rangle,
\end{aligned} \tag{22}
$$

$$
\begin{aligned}
F_{i,j}(t,t') &= \langle\langle S_i^-(t); S_j^-(t')\rangle\rangle \\
&= -i\theta(t - t')\langle[S_i^-(t), S_j^-(t')]\rangle.
\end{aligned} \tag{23}
$$

The equations of motion of these functions read as

$$
\begin{aligned}
i\hbar\frac{dG_{i,j}(t,t')}{dt} &= \langle[S_i^+(t), S_j^-(t')]\rangle\delta(t - t') \\
&\quad - \langle\langle[\mathcal{H}_M, S_i^+]; S_j^-\rangle\rangle
\end{aligned} \tag{24}
$$

$$
\begin{aligned}
i\hbar\frac{dF_{i,j}(t,t')}{dt} &= \langle[S_i^-(t), S_j^-(t')]\rangle\delta(t - t') \\
&\quad - \langle\langle[\mathcal{H}_M, S_i^-]; S_j^-\rangle\rangle.
\end{aligned} \tag{25}
$$

For the $\mathcal{H}_m$ and $\mathcal{H}_a$ parts, the above equations of motion generate terms such as $\langle\langle S_l^z S_i^\pm; S_j^-\rangle\rangle$ and $\langle\langle S_i^\pm S_i^\pm; S_j^-\rangle\rangle$. These functions can be approximated by using the Tyablikov decoupling to reduce to the above-defined G and F functions:

$$
\langle\langle S_l^z S_i^\pm; S_j^-\rangle\rangle \simeq \langle S_l^z\rangle\langle\langle S_i^\pm; S_j^-\rangle\rangle, \tag{26}
$$

$$
\langle\langle S_l^\pm S_i^\pm; S_j^-\rangle\rangle \simeq \langle S_l^\pm\rangle\langle\langle S_i^\pm; S_j^-\rangle\rangle \simeq 0. \tag{27}
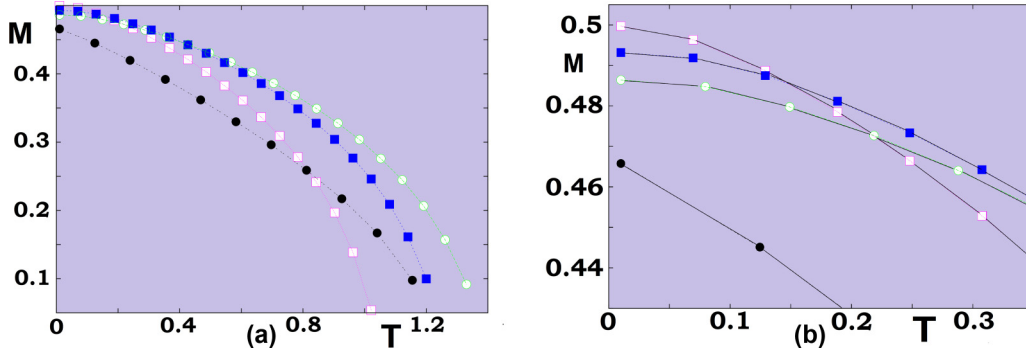$$

FIG. 17. (a) Spin length $M = \langle S^z \rangle$ versus temperature T for a 2D sheet with $\theta = 0.175$ (radian) (magenta void squares), $\theta = 0.524$ (blue filled squares), $\theta = 0.698$ (green void circles), $\theta = 1.047$ (black filled circles). (b) Zoom at low T to show magnetization crossovers.

The last expression is due to the fact that transverse spin-wave motions $\langle S_l^\pm \rangle$ are zero with time. For the DM term, the commutation relations $[\mathcal{H}, S_i^\pm]$ give rise to the following term:

$$D \sum_l \sin \theta \left[\mp S_i^z (S_l^+ + S_l^-) \pm 2 S_i^\pm S_l^z \right]. \tag{28}$$

This leads to the following type of Green's function:

$$\langle \langle S_i^z S_l^\pm ; S_j^- \rangle \rangle \simeq \langle S_i^z \rangle \langle \langle S_l^\pm ; S_j^- \rangle \rangle. \tag{29}$$

Note that we have used defined θ positively. The above equation is thus related to G and F functions [see Eq. (27)].

We use the following Fourier transforms in the xy plane of the G and F Green's functions:

$$G_{i,j}(t, t', \omega) = \frac{1}{\Delta} \int_{BZ} d\mathbf{k}_{xy} e^{-i\hbar\omega(t-t')} g(\omega, \mathbf{k}_{xz}) e^{i\mathbf{k}_{xy} \cdot (\mathbf{R}_i - \mathbf{R}_j)}, \tag{30}$$

$$F_{i,j}(t, t', \omega) = \frac{1}{\Delta} \int_{BZ} d\mathbf{k}_{xy} e^{-i\hbar\omega(t-t')} f(\omega, \mathbf{k}_{xy}) e^{i\mathbf{k}_{xy} \cdot (\mathbf{R}_i - \mathbf{R}_j)}, \tag{31}$$

where the integral is performed in the first xy Brillouin zone (BZ) of surface Δ and ω is the SW frequency. Let us define the SW energy as $E = \hbar\omega$ in the following.

For a monolayer, we have after the Fourier transforms

$$\begin{aligned} (E + A)g + Bf &= 2\langle S^z \rangle, \\ -Bg + (E - A)f &= 0, \end{aligned} \tag{32}$$

where A and B are

$$\begin{aligned} A = &-J^m [8\langle S^z \rangle \cos\theta (1 + d) - 4\langle S^z \rangle \gamma (\cos\theta + 1)] \\ &- 4D \sin\theta \langle S^z \rangle \gamma + 8D \sin\theta \langle S^z \rangle, \end{aligned} \tag{33}$$

$$B = 4J^m \langle S^z \rangle \gamma (\cos\theta - 1) - 4D \sin\theta \langle S^z \rangle \gamma, \tag{34}$$

where the reduced anisotropy is $d = K/J^m$ and $\gamma = (\cos k_x a + \cos k_y a)/2$, k_x and k_y being the wave-vector components in the xy planes, a the lattice constant.

The SW energies are determined by the secular equation

$$\begin{aligned} (E + A)(E - A) + B^2 &= 0, \\ [E + A][E - A] + B^2 &= 0, \\ E^2 - A^2 + B^2 &= 0, \\ E &= \pm \sqrt{(A + B)(A - B)}, \end{aligned} \tag{35}$$

where $\pm$ indicate the left and right SW precessions. We see the following.

(i) If $\theta = 0$, we have B and the last two terms of A are zero. We recover then the ferromagnetic SW dispersion relation

$$E = 2ZJ^m \langle S^z \rangle (1 - \gamma), \tag{36}$$

where $Z = 4$ is the coordination number of the square lattice (taking $d = 0$).

(ii) If $\theta = \pi$, we have $A = 8J^m \langle S^z \rangle$ and $B = -8J^m \langle S^z \rangle \gamma$. We recover then the antiferromagnetic SW energy

$$E = 2ZJ^m \langle S^z \rangle \sqrt{1 - \gamma^2}. \tag{37}$$

(iii) In the presence of a DM interaction, we have $0 < \cos\theta < 1$ ($0 < \theta < \pi/2$). If $d = 0$, the quantity in the square root of Eq. (35) is always $\geqslant 0$ for any θ. It is zero at $\gamma = 1$. We do not need an anisotropy d to stabilize the SW at $T = 0$. If $d \neq 0$, then it gives a gap at $\gamma = 1$.

We show in Fig. 16 the SW energy calculated from Eq. (35) for $\theta = 0.3$ radian ($\simeq 17.2°$) and 1 radian ($\simeq 57.30°$). The spectrum is symmetric for positive and negative wave vectors and for left and right precessions. Note that for small values of θ (i.e., small D) E is proportional to k^2 at low k [cf. Fig. 16(a)], as in ferromagnets. However, for strong θ, E is proportional to k as seen in Fig. 16(b). This behavior is similar to that in antiferromagnets [28]. The change of behavior is progressive with increasing θ, no sudden transition from k^2 to k behavior is observed.

In the case of $S = \frac{1}{2}$, the magnetization is given by (see technical details in Ref. [28])

$$\langle S^z \rangle = \frac{1}{2} - \frac{1}{\Delta} \iint dk_x dk_y \left[\frac{1}{e^{E_i/k_B T} - 1} + \frac{1}{e^{-E_i/k_B T} - 1} \right], \tag{38}$$

where for each $\mathbf{k}$ one has $\pm E_i$ values. Since E_i depends on S^z, the magnetization can be calculated at finite temperatures self-consistently using the above formula.

It is noted that the anisotropy d avoids the logarithmic divergence at $k = 0$ so that we can observe a long-range ordering at finite T in 2D. We show in Fig. 17 the magnetization M ($\equiv \langle S^z \rangle$) calculated by Eq. (38) for using $d = 0.001$. It is interesting to observe that M depends strongly on θ: at high T, larger θ yields stronger M. However, at $T = 0$ the
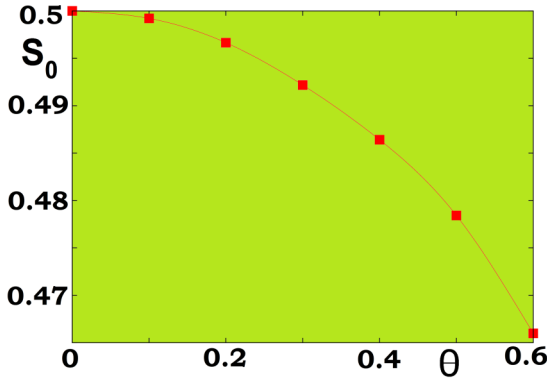
FIG. 18. Spin length at temperature $T = 0$ for a monolayer versus θ (radian).

spin length is smaller for larger θ due to the so-called spin contraction in antiferromagnets [28]. As a consequence, there is a crossover of magnetizations with different θ at low T as shown in Fig. 17.

The spin length at $T = 0$ is shown in Fig. 18 for several θ.

B. Bilayer

We note that for magnetic bilayer between two ferroelectric films, the calculation similar to that of a monolayer can be done. By symmetry, spins between the two layers are parallel, the energy of a spin on a layer is

$$E_i = -4J^m S^2 \cos \theta - J^m S^2 + 4J^{mf} P^z S^2 \sin \theta, \quad (39)$$

where there are four in-plane NN and one parallel NN spin on the other layer. The interface coupling is with only one polarization instead of two [see Eq. (12)] for a monolayer for comparison. The minimum energy corresponds to $\tan \theta = -J^{mf}/J^m$.

The calculation by the Green's functions for a film with a thickness is straightforward: writing the Green's functions for each layer and making Fourier transforms in the xy planes, we obtain a system of coupled equations. For the details, the reader is referred to Ref. [40]. For a bilayer, the SW energy is the eigenvalue of the following matrix equation:

$$\mathbf{M}(E)\mathbf{h} = \mathbf{u}, \quad (40)$$

where

$$\mathbf{h} = \begin{pmatrix} g_{1,n'} \\ f_{1,n'} \\ g_{2,n'} \\ f_{2,n'} \end{pmatrix}, \quad \mathbf{u} = \begin{pmatrix} 2\langle S_1^z \rangle \delta_{1,n'} \\ 0 \\ 2\langle S_2^z \rangle \delta_{2,n'} \\ 0 \end{pmatrix}, \quad (41)$$

where $E = \hbar \omega$ and $\mathbf{M}(E)$ is given by

$$\begin{pmatrix} E + A_1 & B_1 & C_1 & 0 \\ -B_1 & E - A_1 & 0 & -C_1 \\ C_2 & 0 & E + A_2 & B_2 \\ 0 & -C_2 & -B_2 & E - A_2 \end{pmatrix} \quad (42)$$

with

$$A_1 = -J^m \left[8\langle S_1^z \rangle \cos \theta (1 + d) - 4\langle S_1^z \rangle \gamma (\cos \theta + 1) \right] \\ - 2J^m \langle S_2^z \rangle - 4D \sin \theta \langle S_1^z \rangle \gamma + 8D \sin \theta \langle S_1^z \rangle, \quad (43)$$
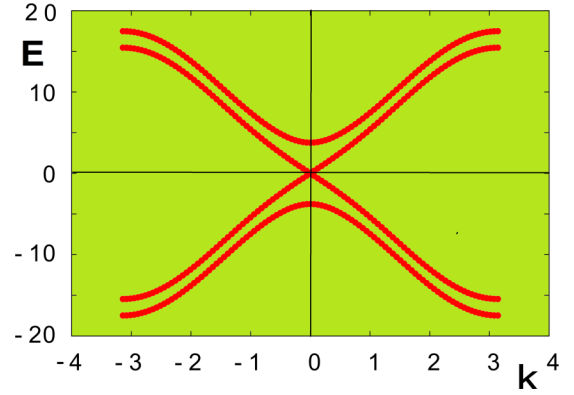

FIG. 19. Spin-wave energy E versus $k = k_x = k_y$ at $T = 0$ for a bilayer with $\theta = 0.6$ radian.

$$A_2 = -J^m \left[8\langle S_2^z \rangle \cos \theta (1 + d) - 4\langle S_2^z \rangle \gamma (\cos \theta + 1) \right] \\ - 2J^m \langle S_1^z \rangle - 4D \sin \theta \langle S_2^z \rangle + 8D \sin \theta \langle S_2^z \rangle, \quad (44)$$

$$B_n = 4J^m \langle S_n^z \rangle \gamma (\cos \theta - 1) - 4D \sin \theta \langle S_n^z \rangle \gamma, \quad n = 1, 2 \quad (45)$$

$$C_n = 2J^m \langle S_n^z \rangle, \quad n = 1, 2. \quad (46)$$

Note that, by symmetry, one has $\langle S_1^z \rangle = \langle S_2^z \rangle$.

We show in Fig. 19 the SW spectrum of the bilayer case for a strong value $\theta = 0.6$ radian. There are two important points: (i) the first mode has the $E \propto k$ antiferromagnetic behavior at the long-wavelength limit for this strong θ; (ii) the higher mode has $E \propto k^2$ which is the ferromagnetic wave due to the parallel NN spins in the z direction.

In conclusion of this section, we emphasize that the DM interaction affects strongly the SW mode at $k \to 0$. Quantum fluctuations in competition with thermal effects cause the crossover of magnetizations of different θ: in general, stronger θ yields stronger spin contraction at and near $T = 0$ so that the corresponding spin length is shorter. However, at higher T, stronger θ means stronger J^{mf} which yields stronger magnetization. It explains the crossover at moderate T.

V. CONCLUSION

We have studied in this paper a model for the interface coupling between a magnetic film and a ferroelectric film in a superlattice. This coupling has the form of a Dzyaloshinskii-Moriya (DM) interaction between a polarization and the spins at the interface. The ground state shows uniform noncollinear spin configurations in zero field and skyrmions in an applied magnetic field. We have studied spin-wave (SW) excitations in a monolayer and in a bilayer in zero field by the Green's function method. We have shown the strong effect of the DM coupling on the SW spectrum as well as on the magnetization at low temperatures.

Monte Carlo simulation has been used to study the phase transition occurring in the superlattice with and without applied field. Skyrmions have been shown to be stable at finite temperatures. We have also shown that the nature of the phase transition can be of second or first order, depending on the DM interface coupling.

The existence of skyrmions confined at the magnetoferro-electric interface is very interesting. We believe that it can be used in transport applications in spintronic devices. A number of applications using skyrmions have been already mentioned in the Introduction.

ACKNOWLEDGMENT

[1] S. Dong, X. Zhang, R. Yu, J.-M. Liu, and E. Dagotto, Microscopic model for the ferroelectric field effect in oxide heterostructures, Phys. Rev. B **84**, 155117 (2011).

[2] M. Mostovoy, Ferroelectricity in Spiral Magnets, Phys. Rev. Lett. **96**, 067601 (2006).

[3] H. Katsura, N. Nagaosa, and A. V. Balatsky, Spin Current and Magnetoelectric Effect in Noncollinear Magnets, Phys. Rev. Lett. **95**, 057205 (2005).

[4] I. A. Sergienko and E. Dagotto, Role of the Dzyaloshinskii-Moriya interaction in multiferroic perovskites, Phys. Rev. B **73**, 094434 (2006).

[5] S.-W. Cheong and M. Mostovoy, Multiferroics: A magnetic twist for ferroelectricity, Nat. Mater. **6**, 13 (2007).

[6] A. Pyatakov, A. Zvezdin, A. Vlasov, A. Sergeev, D. Sechin, E. Nikolaeva, A. Nikolaev, H. Chou, S. Sun, and L. Calvet, Spin structures and domain walls in multiferroics spin structures and magnetic domain walls in multiferroics, Ferroelectrics **438**, 79 (2012).

[7] A. N. Bogdanov and D. Yablonskii, Thermodynamically stable vortices in magnetically ordered crystals. the mixed state of magnets, Zh. Eksp. Teor. Fiz. **95**, 178 (1989) [JETP **68**, 101 (1989)].

[8] A. Bogdanov and A. Hubert, Thermodynamically stable magnetic vortex states in magnetic crystals, J. Magn. Magn. Mater. **138**, 255 (1994).

[9] T. H. R. Skyrme, A unified field theory of mesons and baryons, Nucl. Phys. **31**, 556 (1962).

[10] A. Bogdanov, U. Rößler, M. Wolf, and K.-H. Müller, Magnetic structures and reorientation transitions in noncentrosymmetric uniaxial antiferromagnets, Phys. Rev. B **66**, 214410 (2002).

[11] U. Rößler, A. Bogdanov, and C. Pfleiderer, Spontaneous skyrmion ground states in magnetic metals, Nature (London) **442**, 797 (2006).

[12] H. T. Diep, S. El Hog, and A. Bailly-Reyre, Skyrmion crystals: Dynamics and phase transition, AIP Advances **8**, 055707 (2018).

[13] N. S. Kiselev, A. N. Bogdanov, R. Schäfer, and U. K. Rößler, Chiral skyrmions in thin magnetic films: new objects for magnetic storage technologies? J. Phys. D: Appl. Phys. **44**, 392001 (2011).

[14] J. Sampaio, V. Cros, S. Rohart, A. Thiaville, and A. Fert, Nucleation, stability and current-induced motion of isolated magnetic skyrmions in nanostructures, Nat. Nanotechnol. **8**, 839 (2013).

[15] S. S. Parkin, M. Hayashi, and L. Thomas, Magnetic domain-wall racetrack memory, Science **320**, 190 (2008).

[16] S. Mühlbauer, B. Binz, F. Jonietz, C. Pfleiderer, A. Rosch, A. Neubauer, R. Georgii, and P. Böni, Skyrmion lattice in a chiral magnet, Science **323**, 915 (2009).

[17] W. Münzer, A. Neubauer, T. Adams, S. Mühlbauer, C. Franz, F. Jonietz, R. Georgii, P. Böni, B. Pedersen, M. Schmidt, A. Rosch, and C. Pfleiderer, Skyrmion lattice in the doped semiconductor Fe$_{1-x}$Co$_x$Si, Phys. Rev. B **81**, 041203(R) (2010).

[18] X. Yu, Y. Onose, N. Kanazawa, J. Park, J. Han, Y. Matsui, N. Nagaosa, and Y. Tokura, Real-space observation of a two-dimensional skyrmion crystal, Nature (London) **465**, 901 (2010).

[19] X. Yu, N. Kanazawa, Y. Onose, K. Kimoto, W. Zhang, S. Ishiwata, Y. Matsui, and Y. Tokura, Near room-temperature formation of a skyrmion crystal in thin-films of the helimagnet fege, Nat. Mater. **10**, 106 (2011).

[20] S. Seki, X. Yu, S. Ishiwata, and Y. Tokura, Observation of skyrmions in a multiferroic material, Science **336**, 198 (2012).

[21] S. Seki, S. Ishiwata, and Y. Tokura, Magnetoelectric nature of skyrmions in a chiral magnetic insulator Cu$_2$OSeO$_3$, Phys. Rev. B **86**, 060403(R) (2012).

[22] X. Yu, M. Mostovoy, Y. Tokunaga, W. Zhang, K. Kimoto, Y. Matsui, Y. Kaneko, N. Nagaosa, and Y. Tokura, Magnetic stripes and skyrmions with helicity reversals, Proc. Natl. Acad. Sci. U. S. A. **109**, 8856 (2012).

[23] A. Rosch, Extra twist in magnetic bubbles, Proc. Natl. Acad. Sci. U. S. A. **109**, 8793 (2012).

[24] N. Romming, C. Hanneken, M. Menzel, J. E. Bickel, B. Wolter, K. von Bergmann, A. Kubetzka, and R. Wiesendanger, Writing and deleting single magnetic skyrmions, Science **341**, 636 (2013).

[25] A. Pyatakov, D. Sechin, A. Sergeev, A. Nikolaev, E. Nikolaeva, A. Logginov, and A. Zvezdin, Magnetically switched electric polarity of domain walls in iron garnet films, Europhys. Lett. **93**, 17001 (2011).

[26] W. Koshibae and N. Nagaosa, Theory of skyrmions in bilayer systems, Sci. Rep. **7**, 42645 (2017).

[27] J. Martinez and M. Jalil, Topological dynamics and current-induced motion in a skyrmion lattice, New J. Phys. **18**, 033008 (2016).

[28] H. T. Diep, *Theory Of Magnetism: Application to Surface Physics* (World Scientific, Singapore, 2014).

[29] S. El Hog and H. T. Diep, Partial phase transition and quantum effects in helimagnetic films under an applied field, J. Magn. Magn. Mater. **429**, 102 (2017).

[30] D. P. Landau and K. Binder, *A Guide to Monte Carlo Simulations in Statistical Physics* (Cambridge University Press, Cambridge, 2009).

[31] S. Brooks, A. Gelman, S. L. Jones, and X.-L. Meng, *Handbook of Markov Chain Monte Carlo* (CRC Press, Boca Raton, FL, 2011).

[32] M. Mézard, M. Parisi, and M. Virasoro, *Spin Glass Theory and Beyond: An Introduction to the Replica Method and Its Applications* (World Scientific, Singapore, 1986).

[33] S. El Hog, A. Bailly-Reyre, and H. T. Diep, Stability and phase transition of skyrmion crystals generated by Dzyaloshinskii-Moriya interaction, J. Magn. Magn. Mater. **455**, 32 (2018).

[34] N. D. Mermin and H. Wagner, Absence of Ferromagnetism or Antiferromagnetism in One- or Two-Dimensional Isotropic Heisenberg Models, Phys. Rev. Lett. **17**, 1133 (1966).

[35] D. J. Amit, *Field Theory, the Renormalization Group and Critical Phenomena* (World Scientific, Singapore, 1984).

[36] J. Zinn-Justin, *Quantum Field Theory and Critical Phenomena* (Oxford University Press, Oxford, 2002).

[37] V. T. Ngo and H. T. Diep, Effects of frustrated surface in Heisenberg thin films, Phys. Rev. B **75**, 035412 (2007).

[38] *Frustrated Spin Systems*, 2nd ed., edited by H. T. Diep (World Scientific, Singapore, 2013).

[39] V. T. Ngo and H. T. Diep, Phase transition in Heisenberg stacked triangular antiferromagnets: End of a controversy, Phys. Rev. E **78**, 031119 (2008).

[40] H. T. Diep, Quantum theory of helimagnetic thin films, Phys. Rev. B **91**, 014436 (2015).

[41] S. El Hog, H. T. Diep, and H. Puszkarski, Theory of magnons in spin systems with Dzyaloshinskii-Moriya interaction, J. Phys.: Condens. Matter **29**, 305001 (2017).